To the Graduate Council:

I am submitting herewith a thesis written by Wesley Carlton Parker entitled "Single-Molecule Detection." I have examined the final paper copy of this thesis for form and content and recommend that it be accepted in partial fulfillment of the requirements for the degree of Master of Science, with a major in Physics.

Lloyd M Davis

Dr. Lloyd M. Davis, Major Professor

We have read this thesis
and recommend its acceptance:

Accepted for the Council:

Vice Provost
and Dean of Graduate Studies

Single-Molecule Detection

A Thesis
Presented for the
Master of Science Degree
The University of Tennessee, Knoxville

Wesley C. Parker
May 2002

Acknowledgments

Thanks to my major professor, Dr. Lloyd M. Davis, for his willingness to help, and for his patience. Thanks also to my other committee members, Dr. J. W. L. Lewis and Dr. Christian Parigger, for their helpful comments and assistance on this work. Most of all, thanks to my wife, Anne, without whom none of it would have been possible.

The funding for this project was provided by LI-COR, Inc., and is gratefully acknowledged.

Abstract

Single-molecule detection (SMD) provides a practical method of examining the behavior of individual molecules. This has application both for fundamental studies of particle dynamics such as diffusion in solutions, and for bio-technology applications such as DNA sequencing.

In this thesis I discuss two confocal epi-illumination microscopes constructed at UTSI and used for single-molecule detection and fluorescence correlation spectroscopy. Examples of data collected from experiments using each instrument is presented in which solutions of the fluorescent dye sulforhodamine 101 are analyzed. An example of the use of the instrument to detect fluorescence quenching is also presented.

Contents

List of Figures

List of Tables

Chapter 1

Introduction

1.1 Previous experiments in single-molecule detection in solution

The detection of single molecules in solution by optical means was first reported by Hirschfeld in 1976 [1]. Hirschfeld was able to detect individual molecules of gamma globulin bound to one molecule of polyethyleneimine, to which was attached between eighty and one hundred molecules of the fluorescent dye fluorescein. The fluorescein molecules were excited by an argon laser, and the resulting fluorescence was detected using a photomultiplier tube. During detection complete photobleaching of the fluorescein molecules occurred.

Subsequent enhancements in single-molecule detection (SMD) methods would employ single photon avalanche diodes (SPADs) in place of photomultiplier tubes to increase light-detection sensitivity and reduce noise, and would achieve smaller sample volumes in order to minimize the background from solvent of Raman scatter and impurity fluorescence. Data analysis made use of the autocorrelation function to determine whether light fluctuations characteristic of small numbers of molecules were being ob-

served [2]. At that point, single-molecule detection was typically accomplished through the observation of fluorescence from a number of chromophores attached to a larger molecule, and as those large molecules traveled through the detection region, their presence was determined statistically by the autocorrelation function.

In 1990, the use of excitation from a pulsed laser with high repetition rate allowed a research group at Los Alamos National Laboratory to report the detection of individual single-chromophore molecules of rhodamine 6G (R6G) dye molecules. The R6G molecules were in a 10^{-13} M concentration in an aqueous solution. Time-gated detection was used to discriminate against Raman scattered light, and a digital filter allowed the researchers to identify photon bursts from individual dye molecules [3].

Recent developments here at UTSI have focused on the evaluation of SPAD detectors [4], the development of Monte Carlo simulation software to model sample behavior in flow cells and the development of flow systems that yield the most efficient detection of single molecules [5], simulations of SMD experiments [6], and the use of neural networks to analyze the results of SMD experiments [7].

1.2 Benefits of single-molecule detection

Once individual molecules are detected, rather than the average behavior of a group of molecules, it becomes possible to investigate the physical properties of individual molecules. Instruments which can detect molecules on an individual basis allow more insight into questions about molecular spectra, the fluorescent lifetimes of molecular species, and the dynamics of diffusion.

By its nature, SMD offers an extremely sensitive tool for chemical analysis. A typical application of SMD in the bio-sciences is to tag biological molecules with fluorescent labels and pass them through a flow cell. While in the flow cell, the fluorescent tags are excited by a laser, and the resulting fluorescence is collected by a detection system. This technique has become the basis of efforts to sequence DNA in a rapid manner.

Chapter 2

Principles of single-molecule detection

The technique used in this work has four steps: (1) fluorescence is induced in the sample by means of laser excitation; (2) light emitted from the sample is collected onto a SPAD detector; (3) the photon counts from the SPAD are digitized and stored on a computer; and (4) the digitized data is analyzed using various software routines.

The first step in this technique is based on the process of fluorescence, illustrated in Figure 2.1. Molecules may absorb a photon of light and become electronically excited to a rotationally and vibrationally excited sublevel of the singlet S1 energy band. Thermal relaxation to the ground ro-vibrational level of the S1 manifold occurs after about 1 picosecond. The molecule may then return to the ground state by a number of different mechanisms. The most direct method is by a dipole transition accompanied by emission of a photon. This process is called fluorescence, and it occurs after an interval of about a few nanoseconds. The molecule may also return to the ground state indirectly, by first decaying non-radiatively to the triplet state, and then to the ground state. If this

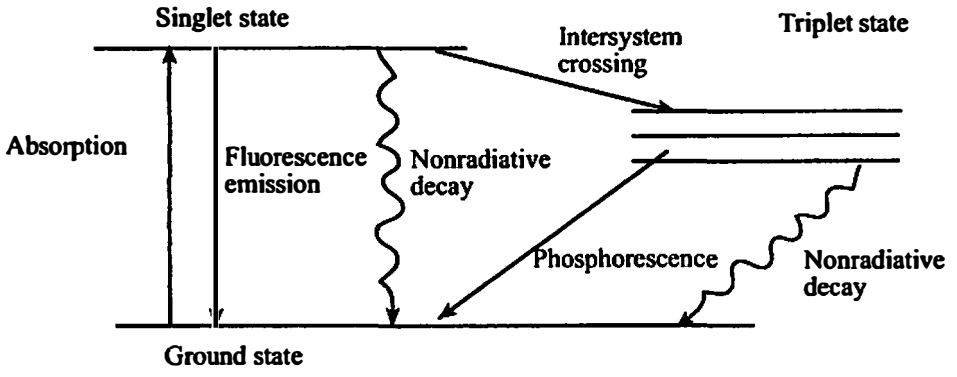

Figure 2.1: Fluoresence emission and competing processes

decay process is accompanied by a photon it is called phosphorescence, and it occurs on the order of 10^{-6} second to 10^{-1} seconds. In addition to these radiative processes, the molecule may return to the ground state by nonradiative decay from collisional interactions with solvent or other molecules or by heat dissipation [8].

Fluorophores may be characterized by excitation and emission spectra, fluorescence lifetime, which is the mean time the molecule stays in the excited singlet state, photobleaching properties, and diffusion coefficients. Naturally occurring fluorophores include aromatic amino acids, nicotinamide adenine dinucleotide (NADH), flavins, and derivatives of pyridoxal and chlorophyll. Fluorophores that have been developed in the laboratory include dansyl chloride, fluorescein, and various rhodamines. It is important to note that not all molecules fluoresce [9].

In our experiments, we induce fluorescence in the sample by using a laser to excite the molecule. The laser may either be a pulsed or a continuous wave laser. Pulsed

lasers allow time-gated detection; continuous wave lasers allow the fluorophores to be re-excited immediately after decay to the ground state. In either case, the optimum wavelength of the laser used to excite the fluorophore will depend on the peak absorption wavelength of the particular fluorophore.

Depending on the objectives of the experiment, there are a number of ways to deliver the beam to the sample and collect the resulting fluorescence. In our experiments, we utilize a confocal epi-illumination configuration. With epi-illumination, laser light is focused on the sample through a microscope objective and the resulting fluorescence is collected by the same objective. With confocal detection, the collected light is focused on a pinhole, which acts as a spatial filter to define the sample volume. The size of the pinhole is selected to define a sample volume that is as small as possible, within the diffraction limit of the microscope objective, so as to minimize the amount of background light that is collected. The light that passes through the pinhole is focused onto a detector. Before the light reaches the detector, it is spectrally filtered to reduce background.

There are different sources of background that can overwhelm the weak fluorescence signal of a single molecule. In addition to containing fluorescence from the sample, the collected light also contains Rayleigh scattered and Raman scattered light from the solvent, specular scatter from optical interfaces, ambient light, fluorescence from optical components in the system, and possibly fluorescence from contaminants in the sample itself. These various sources of background need to be decreased as much as possible.

Generally, background due to Rayleigh scatter may be minimized or eliminated by the use of a Raman notch filter, which blocks the laser wavelength with an optical density of about 6-7. These filters get their name from their use in Raman spectroscopy. A bandpass filter is also used to attenuate the amount of solvent Raman-scatter. Spatial filters help to minimize the effect of specular scatter from optical components. Autofluorescence background from optical components may also be reduced by selecting fused silica optical substrates.

2.1 Scope of this work

Two confocal epi-illumination microscopes were constructed at UTSI to obtain measurements of fluorescence quenching and to determine the photophysical properties of certain fluorescent probes. The first of these instruments, which I refer to as the UTSI instrument, was constructed shortly before I became involved with this project. I used this instrument to take extensive amounts of data for a contract research project funded by LI-COR, Inc. The purpose of the project was to examine the effect of fluorescence quenching on various undisclosed fluorophores.

I assisted in the construction of a second confocal microscope, which I refer to in this thesis as the LI-COR instrument. This instrument was constructed as part of a separate research contract with LI-COR. This instrument was delivered to LI-COR shortly after construction, and it was not used for substantial measurements before its delivery.

A discussion of the design and construction of these two instruments will be found in Chapter 2. Chapter 3 will review the autocorrelation function, and will discuss how it

is used in determining certain photophysical properties of the molecules in the solution. Chapter 4 will discuss the results of experiments which compare the performance of the two instruments. An example of the use of the UTSI confocal microscope to investigate fluorescence quenching will also be presented. Chapter 5 will present experiments on single-molecule imaging in which I was involved.

Chapter 3

Hardware

3.1 UTSI instrument

The first instrument constructed at UTSI utilizes a frequency-doubled mode-locked Coherent Antares Nd:YAG laser to provide 70 ps pulses of 532 nm at a repetition rate of 76 MHz. The Nd:YAG laser pumps a Coherent 702-1 dye laser using rhodamine 6G, which yields laser wavelengths from 570 to 610 nanometers. This laser is tuned to provide 585 nm output pulses, which is the appropriate excitation wavelength for the dye molecule SR-101. The dye laser pulses are on the order of a few picoseconds in width, and are produced at a repetition rate of 76 MHz. The laser beam emerges with vertical polarization and then passes through a gradient neutral-density filter, which can be adjusted to deliver the required laser power, as seen in Figure 3.1.

Using a pulsed mode-locked laser allows fluorescence lifetimes to be determined through the use of time-resolved photon detection. When the sample is repetitively excited, light scattered from the sample and any light with a fluorescence lifetime on the order of a nanosecond will be recorded almost synchronously with each laser pulse.

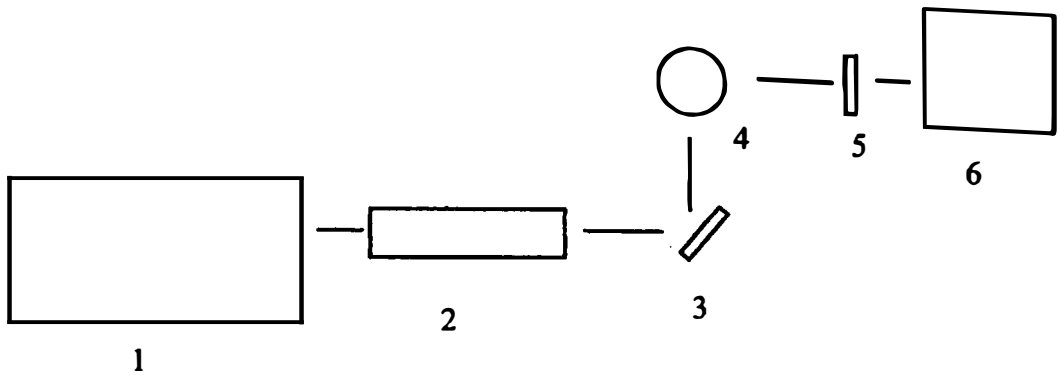

1. Nd:YAG laser
2. Pulsed dye laser
3. Mirror
4. Periscope
5. Filter
6. Confocal microscope

Figure 3.1: UTSI optics configuration

Fluorescence photons from the chromophores attached to the sample molecules will also be recorded, but these will be delayed by the fluorescence lifetime of the dye, which is typically 3-4 nanoseconds.

The polarization state of the beam emerging from the dye laser is changed to horizontal by passing the beam through a periscope mirror arrangement. The beam is then focused by a lens and passed into the microscope, which is surrounded by a light-tight box to prevent room light and scattered laser light from entering the instrument. Changing the polarization of the beam to horizontal makes it s-polarized with respect to the pelical beam splitter contained within the confocal microscope, thereby maximizing the reflectance of the beam.

The pelical beam splitter is used to direct the beam into a microscope objective, as

seen in Figure 3.2. The pelical beam splitter thickness was selected by the manufacturer to give peak reflectance (16%) at 585nm at 45° for s-polarization. The transmitted portion of the laser beam is blocked by a beam dump.

The microscope objective is a Nikon model 190646 oil immersion objective, with a lateral magnification of 100x and an numerical aperture (NA) of 1.3. The excitation beam is focused by the objective to a beam waist of about 0.5 microns in an aqueous sample on a microscope coverslip supported above the objective. Fluorescence from the sample is collected by the same objective, directed back through the beam splitter, and focused through a 100 micron diameter pinhole. This serves as a spatial filter, defining a cylindrical probe region with a volume of about 0.5 femtoliters. The beam is focused into the sample so that the probe region is no more than 25 microns from the boundary formed by the coverslip.

The amount of light that the objective can collect is determined by the numerical aperture of the objective and the index of refraction of the immersion media. The numerical aperture is defined as

$$\text{N.A.} = n \sin\theta \,, \tag{3.1}$$

where n is the index of refraction of the immersion media. in the space between the microscope objective and the lens, and θ is half the collection angle. Assuming that light is collected from a point very close to the surface of the coverslip and that fluorescence is emitted isotropically into a solid angle of 4π, the light collection efficiency is

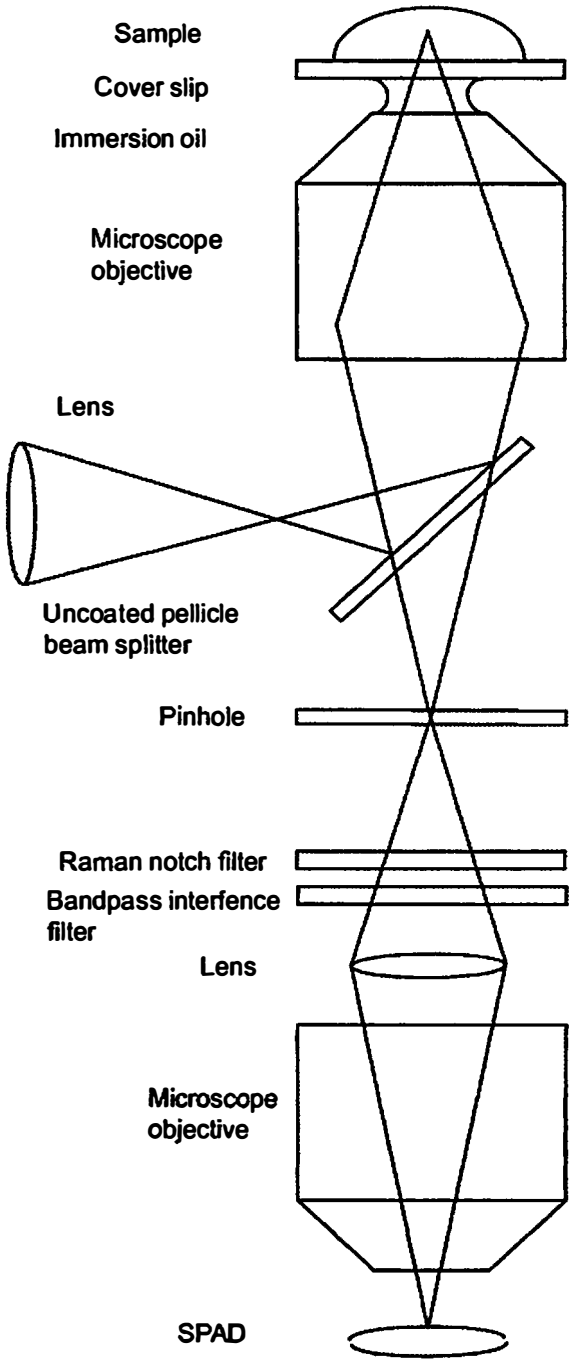

Figure 3.2: UTSI microscope optics

$$\text{collection efficiency} = \sin^2(\theta/2) \ . \tag{3.2}$$

With this particular microscope objective, the immersion oil used has an index of refraction of 1.515, so that $\theta = 59°$ and the collection efficiency is at most 0.24.

Figure 3.3 illustrates the normalized fluorescence emission spectrum of SR101, the transmission of the bandpass interference filter, and the optical density of the Raman notch filter. Once the collected light passes through the pinhole, a Raman notch filter is used to reject Rayleigh light scatter. A band-pass interference filter (Chroma, Inc.) is then used to block Raman scatter from the solvent and also stray fluorescence from outside the band of the fluorophore used to mark the sample. Note that this band-pass filter has zero spectral overlap with the laser line filter shown in Figure 3.1, which serves to block broadband dye-laser luminescence from the excitation beam. These steps ensure that the fluorescence we detect is due only to that from the sample molecule of interest.

After passing through the filters, the fluorescence is focused onto an EG&G SPCM-AQ SPAD detector. This is an actively quenched SPAD with a maximum count rate of 12 MHz, and a dead time of 65 ns.

The use of a pulsed mode locked laser allows time-gated detection. When the sample is repetitively excited, light scattered from the sample and any fluorescence characteristic of the sample with a fluorescence lifetime of less than a nanosecond will be recorded almost synchronously with each laser pulse. Fluorescence photons from the

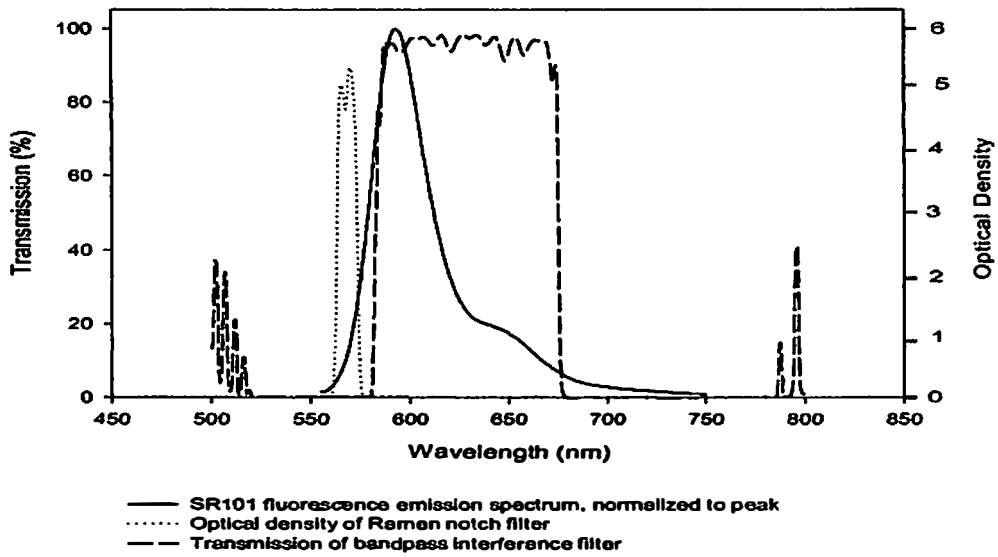

Figure 3.3: Filter transmission curves for use with sulforhodamine 101

chromophores. These will be delayed by the fluorescent lifetime of the dye, typically an average of 3 to 4 nanoseconds.

Figure 3.4 illustrates the data acquisition arrangement of the UTSI instrument for a typical fluorescence lifetime experiment. Laser light from the dye-laser is split into two paths, one of which is directed into the microscope resulting in fluorescence signal, which is focused on the SPAD, as discussed above. The output signal from the SPAD passes through a constant fraction discriminator (CFD), which generates a standard negative pulse for the "start" input to the time-to-amplitude converter (TAC). The other dye laser beam falls upon a fast photodiode. The output from this passes to

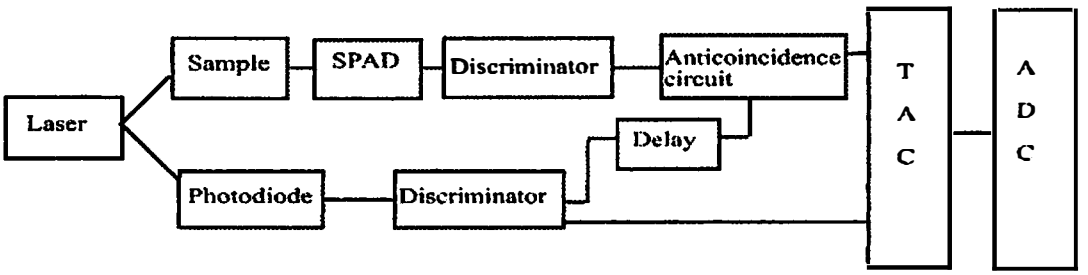

Figure 3.4: UTSI electronics and data acquisition

another CFD, which generates the "stop" input for the TAC. The TAC converts the time duration between "start" and "stop" pulses into an output pulse whose amplitude is proportional to the time interval. Output from the TAC is digitized by an analog-to-digital converter within a PC. Evaluation of the autocorrelation function was then performed using custom software, as described more fully in Reference [5].

3.2 LI-COR instrument

The second instrument utilizes a Spectra Physics continuous wave argon/krypton laser to provide a light source, as shown in Figure 3.5. A laser wavelength of 568 nanometers was used for our experiments. Using a continuous wave laser does not allow for time-gated detection, since the sample is continuously illuminated.

As noted earlier, laser power for the UTSI microscope was adjusted by monitoring the output of a photodiode and adjusting a neutral density gradient filter until the

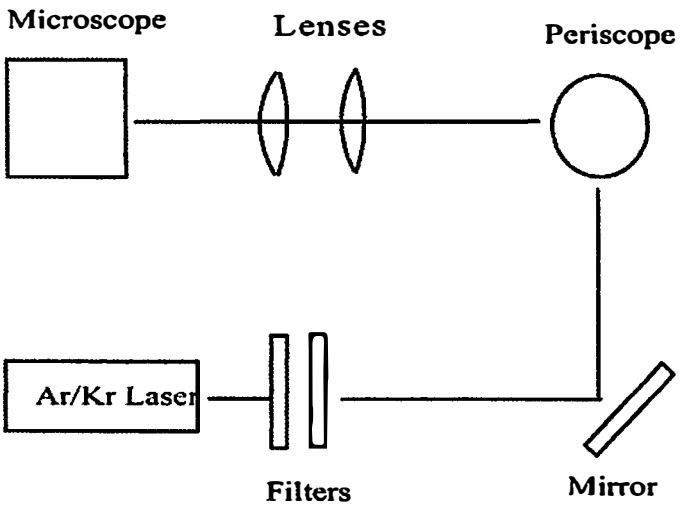

Figure 3.5: LI-COR optics configuration

desired power level was obtained. This procedure was managed differently for the LI-COR instrument. The laser was directed through two selected fixed ND filters onto a power meter, and the laser current was then varied until the desired power was obtained.

The laser beam emerges from the argon/krypton laser vertically polarized. The polarization state is changed to horizontal by passing the beam through a mirror arrangement similar to that used with the first instrument. The beam is then expanded three-fold by a pair of lenses, and passed into the microscope. The LI-COR instrument was constructed so that the optical paths were contained within a set of light-tight tubes with nonreflective walls. A light-tight sample box and fitting for the beam splitter were constructed in our machine shop to complete the assembly of light-tight components.

An uncoated fused-silica beam splitter directs the beam into a Zeiss 1.2 NA water

immersion microscope objective, as seen in Figure 3.6. Using the expressions in equations 1 and 3.2, with $n = 1.33$ for water, the maximum collection efficiency of this objective is 0.28.

As with the UTSI instrument, the excitation beam is then focused to a beam waist of about 0.5 microns in a sample on a microscope coverslip supported above the objective. Fluorescence from the sample is collected by the same objective, directed back through the beam splitter, and focused by a 165.5mm tube lens through an 80 micron pinhole. The beam is focused in the sample area so that the probe region is far from the boundary formed by the coverslip. In this way autofluoresence from the glass coverslip is effectively blocked by the spatial filter. Once the collected light passes through the pinhole it is passed through a Raman notch filter and an interference filter, similar to those in the UTSI instrument. After passing through the filters, the fluorescence is focused onto an EG&G SPCM-PQ passively quenched SPAD detector with a maximum count rate of about 1 MHz and a dead time of 800 ns.

As shown in Figure 3.7, the signal from the SPAD, which consists of millivolt pulses, is conditioned to produce TTL (+5V) pulses for input to a multichannel scalar (MCS) board. For this purpose a Tektronix 7104 oscilloscope was used as a leading edge discriminator, and TTL pulses were provided by the gate output of the oscilloscope. The MCS was contained within a personal computer, and the autocorrelation function was performed by means of a custom software program.

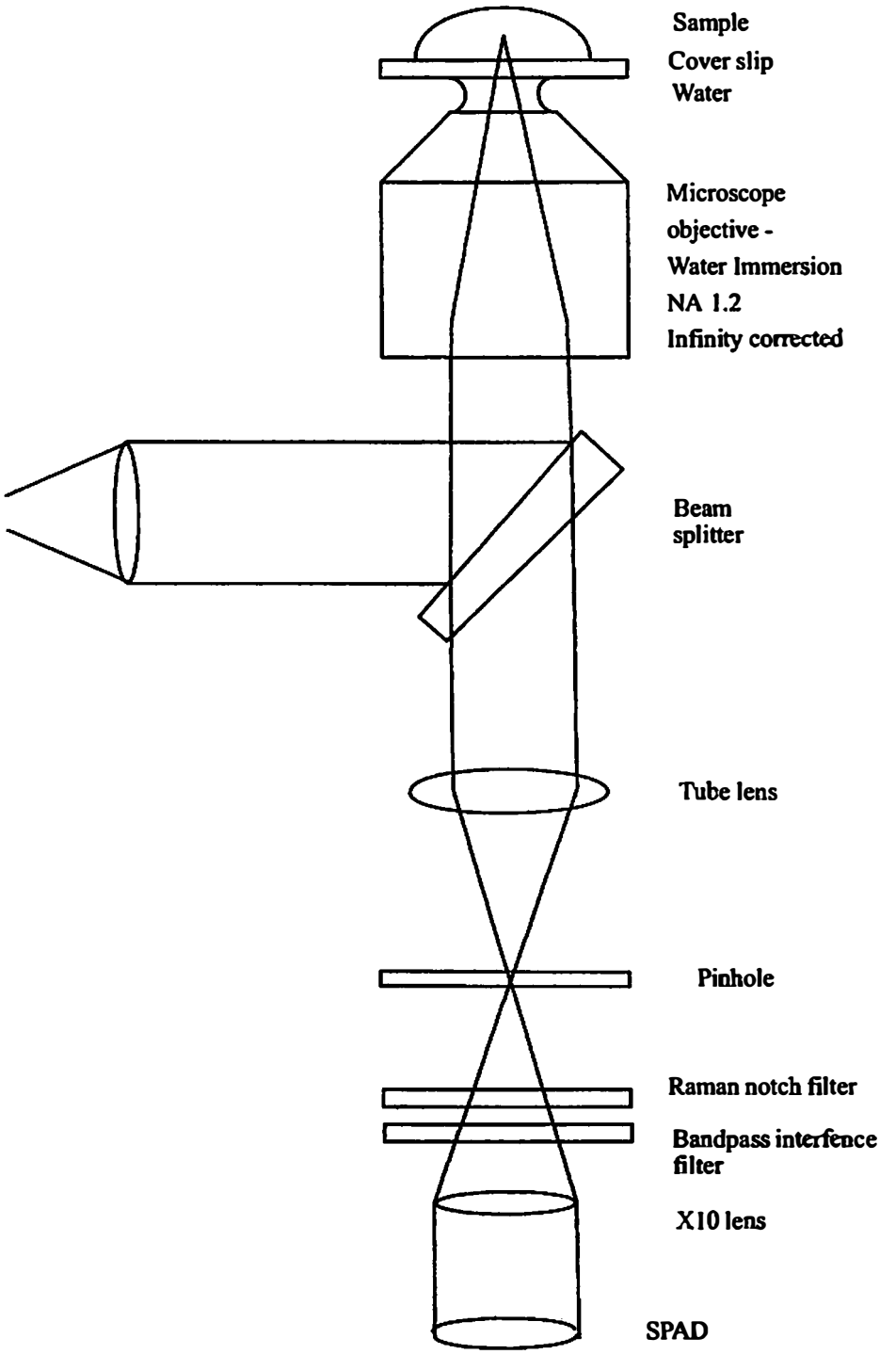

Figure 3.6: LI-COR microscope optics

Figure 3.7: LI-COR electronics and data acquisition

Chapter 4

Data analysis

4.1 Autocorrelation function

The autocorrelation function is defined as

$$G(\tau) = < I(t)I(t+\tau) > \tag{4.1}$$

$$= \int_{-\infty}^{\infty} I(t)I(t+\tau)\,dt\ , \tag{4.2}$$

where $I(t)$ is the signal intensity at time t. If photons occur at random intervals and no molecules pass through the probe volume, then we expect the autocorrelation function to be flat, except for a peak at the point $\tau = 0$. If molecules pass through the sample volume and we observe photon bursts, then the autocorrelation function will include a broad peak about $\tau = 0$.

When data is collected at discrete times during an experiment of finite duration, the autocorrelation function may be expressed as:

$$G(\tau) = \sum_{n=0}^{n=end} I(n)I(n+\tau)\,, \tag{4.3}$$

where $I(n)$ is the signal intensity at time $n = 0, 1, 2, ..., end$. The autocorrelation function is a sensitive indication of the presence of molecules even if the photon bursts are relatively small compared with the mean intensity, because the summation is performed over the entire duration of the experiment.

In the present experiments we are accumulating photon counts. If one expresses the photons counted in the nth channel of the MCS board as $P(n)$, taking into account that the MCS board has 4096 channels so that $n = 0, 1, \ldots, 4095$, one may write

$$G(m) = \sum_{n=0}^{4095-k} P(n)P(n+m)\,, \qquad m = 1, 2, \ldots, k\,, \tag{4.4}$$

where k represents the maximum delay over which the autocorrelation is calculated. For example, if the dwell time for each channel of the MCS is 200 μs, and the value of k is 50, then the autocorrelation is evaluated out to a maximum of 10 milliseconds.

In these experiments, data is collected in a series of i sets. This occurs because the data acquisition program works by filling a buffer with the data accumulated in the 4096 channels of the MCS board, then writing that data sequentially into a data file. This write operation interrupts data collection. We adjust the calculation of the autocorrelation function accordingly by calculating the autocorrelation function for the i-th data set, then summing over the sets of data to obtain an unnormalized autocorrelation function given by

$$G(m) = \sum_{i} \sum_{n=0}^{4095-k} P_i(n) P_i(n+m)\,, \tag{4.5}$$

and the value of the autocorrelation function at $m = 0$ is given by

$$G(0) = \sum_{i} \sum_{n=0}^{4095-k} P_i(n) P_i(n)\,. \tag{4.6}$$

At this point, we want to normalize the autocorrelation function. We write the normalized autocorrelation function as

$$g(\tau) = \frac{< I(t) I(t+\tau) >}{< I(t) >< I(t+\tau) >} \tag{4.7}$$

$$= \frac{\int_{-\infty}^{\infty} I(t) I(t+\tau)\, dt}{\int_{-\infty}^{\infty} I(t)\, dt \int_{-\infty}^{\infty} I(t+\tau)\, dt}\,. \tag{4.8}$$

In the context of our experiment, this becomes

$$g(m) = \frac{(4096-k) \sum_{n=0}^{4095-k} P(n) P(n+m)}{(\sum_{n=0}^{4095-k} P(n))\,(\sum_{n=0}^{4095-k} P(n+m))}\,, \tag{4.9}$$

for each if the i-th data sets.

4.2 Photon burst amplitudes

The autocorrelation function is used in fluorescence correlation spectroscopy to determine diffusional and photochemical dynamics of small numbers of molecules within the probe volume, but it is not sufficient to indicate whether we have observed a single molecule transit the probe volume. In this case we need to generate a burst signal

that corresponds to the presence of a single molecule. A simple way to process the data is to apply a sliding sum to the data stream over a fixed time interval equal to the mean diffusional residence time. These counts per time interval are accumulated for the duration of the experiment. The peak amplitudes are then determined, and a histogram of the peak amplitudes is plotted against the number of peaks. Finally, a cumulative histogram plotting the number of peaks smaller than the peak amplitude is plotted against the peak amplitude.

4.3 Curve-fitting

4.3.1 Translational diffusion

The autocorrelation function that we obtained from the experiment not only indicates whether we are able to detect single molecules, it gives us information about certain photophysical properties of the molecules. In 1976 Aragón and Pecora showed theoretically that for diffusion of molecules through an ellipsoidal volume, the normalized autocorrelation function takes the functional form

$$g(t) = 1 + \frac{1}{N}(1 + \frac{4\,D\,t}{\omega_o^2})^{-1}(1 + \frac{4\,D\,t}{z_o^2})^{-\frac{1}{2}}\,, \tag{4.10}$$

where N depends on the mean number of dye molecules in the probe volume, ω_o is the radius of the probe volume, z_o is the axial radius of the probe volume, and D is the translational diffusion coefficient of the molecule [10].

This form of the equation contains four variables, but only three are independent variables. We make the following substitutions:

$$a_1 = \frac{1}{N}, \tag{4.11}$$

$$a_2 = \frac{D}{\omega_o^2}, \tag{4.12}$$

$$a_3 = \frac{\omega_o^2}{z_o^2}. \tag{4.13}$$

After making these substitutions, the functional form of the autocorrelation function (4.10) becomes

$$g(t) = 1 + a_1(1 + 4\,a_2\,t)^{-1}(1 + 4\,a_2\,a_3\,t)^{-\frac{1}{2}}. \tag{4.14}$$

The above equation makes two assumptions; that the probe volume is a three dimensional Gaussian ellipse of radius ω_o and axial radius z_o; and that fluorescence fluctuations are due primarily to the translational diffusion of molecules through the probe volume. The first assumption is appropriate for a confocal epi-illumination microscope.

4.3.2 Translational diffusion with triplet-state effects

The second assumption becomes invalid when intersystem crossing and triplet-state depopulation occur [11]. When this is taken into account, equation (4.14) is modified by taking into account the rate constants for the excitation and de-excitation of the singlet state (k_{12} and k_{21}), intersystem crossing (k_{23}), and de-excitation of the triplet state(k_{31}). Letting λ reflect the rate at which the triplet-state is populated, we have

$$\lambda = -k_{31} - \frac{k_{12}\,k_{23}}{k_{12} + k_{21}}. \tag{4.15}$$

At equilibrium, the population in the triplet state is

$$T_{eq} = \frac{k_{12}\, k_{23}}{k_{12}(k_{23} + k_{31}) + k_{31}(k_{21} + k_{23})} \tag{4.16}$$

As shown in Reference [11], we may then modify (4.14) to reflect these effects :

$$g(t) = 1 + a_1(1 + 4\, a_2\, t)^{-1}(1 + 4\, a_2\, a_3\, t)^{-\frac{1}{2}} \times (1 - T_{eq} + T_{eq}\, e^{\lambda t}) \; . \tag{4.17}$$

The result of triple state crossing effects on the graph of experimental data is that an additional smaller peak is observed near the origin in the graph of the autocorrelation function.

Chapter 5

Experimental results

5.1 Overview

Experiments were performed to compare the two instruments using sulforhodamine 101 (SR101), a fluorescent molecule available from Sigma, with parameters shown in Table 5.1 [12].

In the first set of experiments, 0.00239 g of SR101 was combined with 2 ml methanol and 8 ml of triple distilled water to yield a 3.94×10^{-4} M solution. The solution was then serially diluted to give samples ranging from 10^{-5} to 10^{-11} M.

Table 5.1: Photophysical properties of sulforhodamine 101

Fluorescent molecule	SR101
Absorption cross-section ($\times 10^{-16} cm^2$)	3.7
Extinction ($cm^{-1}M^{-1}$)	108,000
Molecular weight (g/m)	606.71
Absorption maximum (nm)	586
Emission maximum (nm)	605
Fluorescence quantum yield	0.35
Fluorescence lifetime (ns)	4.2
Photobleaching quantum efficiency ($\times 10^{-5}$)	5.5

5.2 Single-molecule detection experiment using the LI-COR instrument

Once the samples of SR101 was prepared, 90 μl triple distilled water (Carolina Biological Supply Company) was placed on the microscope coverslip in the LI-COR instrument and tested to ensure that no fluorescence was detected by the microscope. Once that was done, 10 μl of 10^{-11} M SR101 was added to the fused silica coverslip, yielding a 10^{-12} M solution. Similar procedures were used to test samples of 10^{-11} and 10^{-10} M.

The sample was loaded on the coverslip and the laser beam back-reflected from the coverslip/sample interface was focused on the pinhole, utilizing a Edmund pocket microscope mounted in such a way as to view the pinhole. The input laser beam alignment was adjusted so that the back-reflection of the laser from the coverslip surface was exactly focused on the pinhole, then the coverslip was moved down 25 microns. This procedure helped eliminate fluorescence from the coverslip. The laser current was adjusted to 26 A, which resulted in less than a milliwatt of laser power at the sample.

Figures 5.1, 5.2 and 5.3 are plots of the autocorrelation function of various samples of SR101 examined using the LI-COR instrument. In each case the normalized autocorrelation function of the experimental results is plotted by the dotted line, and the solid line represents the autocorrelation function fitted using SigmaPlot 2000's non-linear regression routines. The standard deviations of the data points are not known, and hence unweighted curve fitting is used, as is the common practice [13].

The fitting coefficients of equation 4.14 are listed in table 5.2. As discussed earlier,

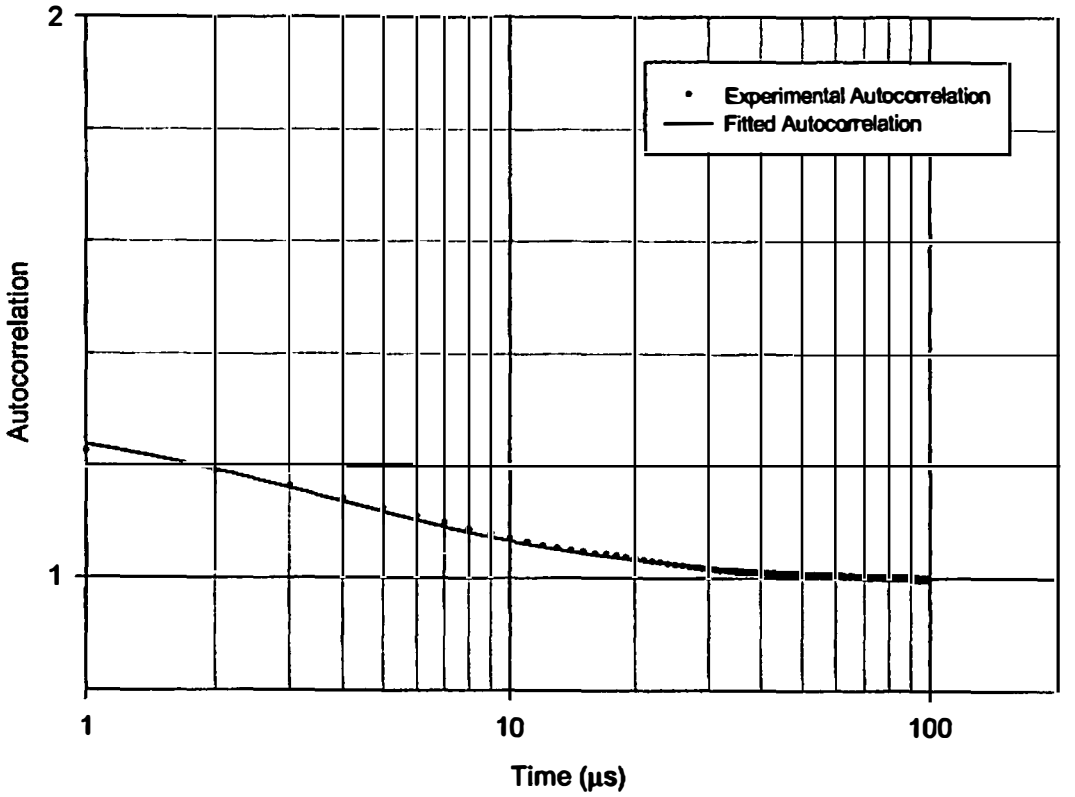

Figure 5.1: Autocorrelation fitting, 10^{-12}M sample

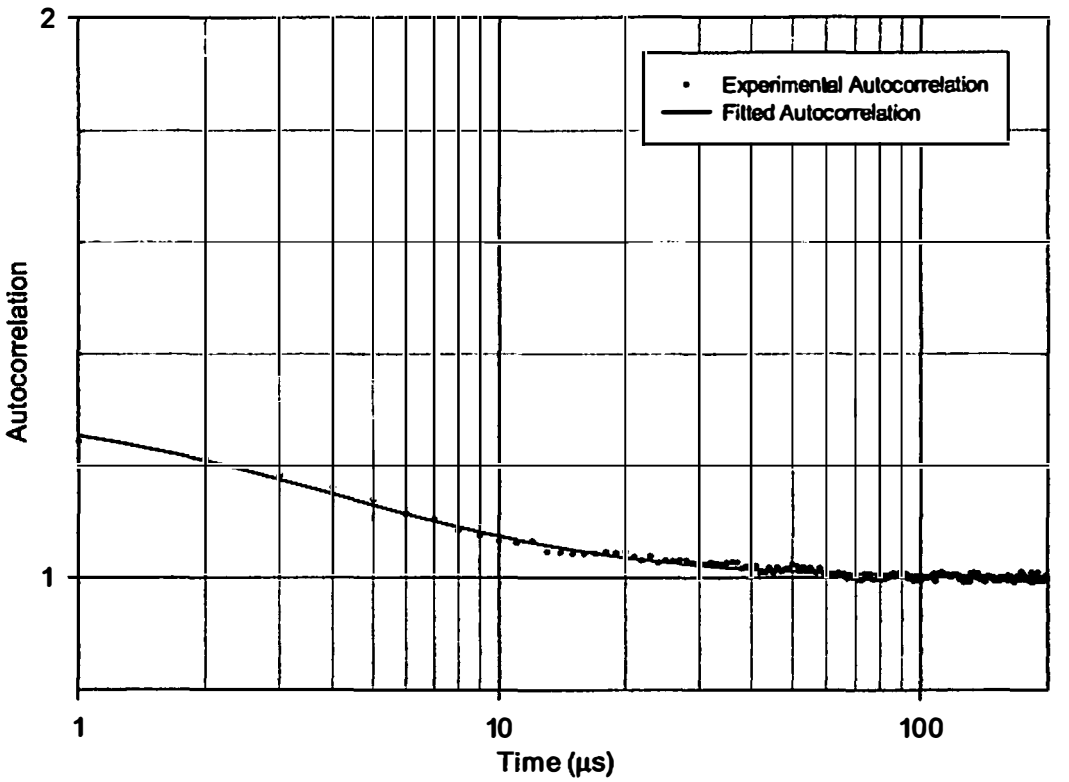

Figure 5.2: Autocorrelation fitting, 10^{-11}M sample

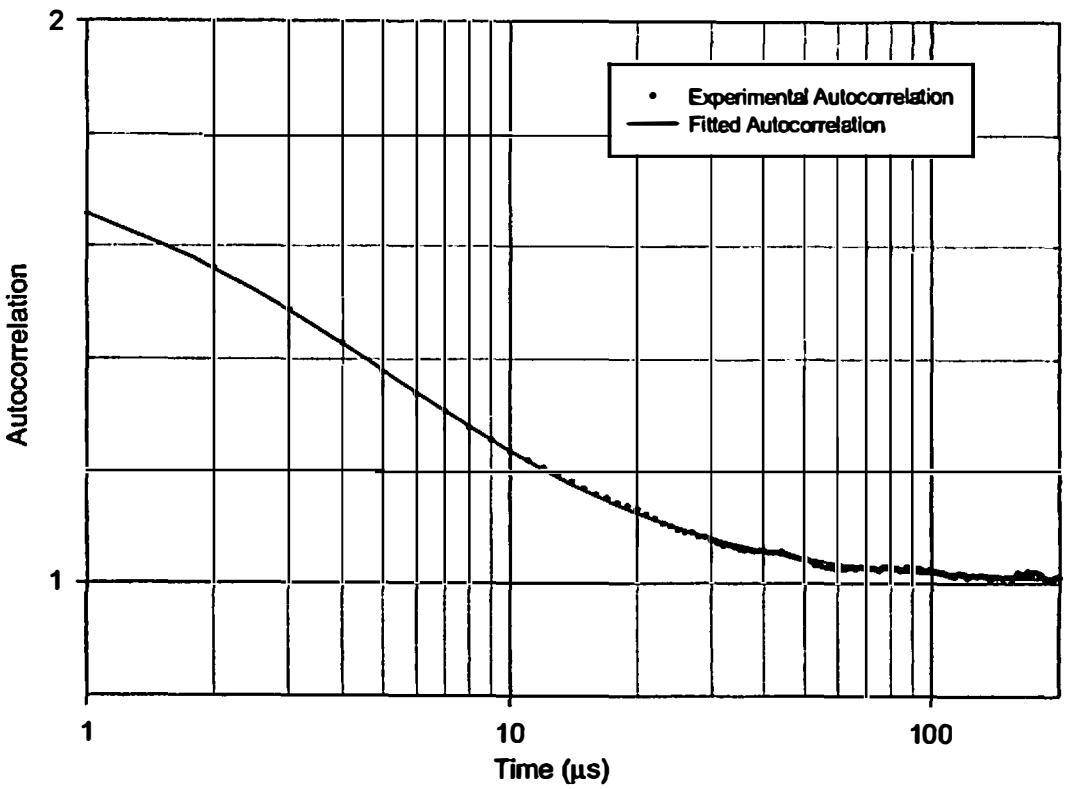

Figure 5.3: Autocorrelation fitting, 10^{-10}M sample

the a_1 coefficient reflects the amplitude of the autocorrelation curve. We see that as the molarity of the samples increase, the amplitude of the signal increases, which is to be expected.

The a_2 coefficient expresses the ratio of the diffusion coefficient to the square of the width of the sample volume. It represents the mean diffusional residence time of a molecule with diffusion coeeficient D within a sphere of radius ω_0. We expect this value to be constant regardless of the molarity of the sample, and this appears to be the case.

The a_3 coefficient represents the ellipticity of the sample volume, equal to the radial width of the sample volume squared divided by the radial length of the sample volume squared. We expect this number to be less than one because the sample volume is a prolate Gaussian ellipsoid.

No additional peaks were observed in the examination of the experimental autocorrelation function, so fitting for triplet state effects was not performed.

5.3 Single-molecule detection experiment using the UTSI instrument

Two samples of SR101 of 10^{-11} and 10^{-9} M were examined using the UTSI instrument. A similar procedure as used in the LI-COR instrument was used to prepare and view

Table 5.2: Autocorrelation fitting coefficients (LI-COR instrument)

Sample	a_1	a_2 (s^{-1})	a_3
10^{-12} M	0.30	0.04	1.00
10^{-11} M	0.32	0.04	0.98
10^{-10} M	0.79	0.04	0.31

the samples.

Figures 5.4 and 5.5 are plots of the autocorrelation function of various samples of SR101 examined using the UTSI instrument. As before, the normalized autocorrelation function of the experimental results is plotted by the dotted line, and the solid line represents the fit to the autocorrelation function using SigmaPlot 2000's non-linear regression routines. The fitting coefficients for these samples are listed in Table 5.3.

In these experiments, the autocorrelation fit was good, but the results were not what was originally expected. As the sample molarity increased, the amplitude of the peak, a_1, actually decreased slightly. Also, the a_2 coefficients were not the same, and the sample volume appeared to be spherical rather than ellipsoidal.

The use of an oil-immersion objective with the UTSI instrument gives rise to spherical aberration in the optics due to refraction at the coverslip/sample interface, which is not corrected by the objective, and this may lead to a sample volume that is more spherical than that of the LI-COR instrument.

Note also that the laser power varied between the two experiments, and hence the results raise the question of how laser power affects the autocorrelation function. It would be of interest to perform a series of experiments with this (or a similar) confocal microscope and laser arrangement in which the laser power was monitored and increased stepwise for each series of experiments. [Such a series of experiments has recently been conducted by David Ball at UTSI. The amplitude of the peak in the autocorrelation was indeed observed to decrease with laser power. Computer simulations conducted by

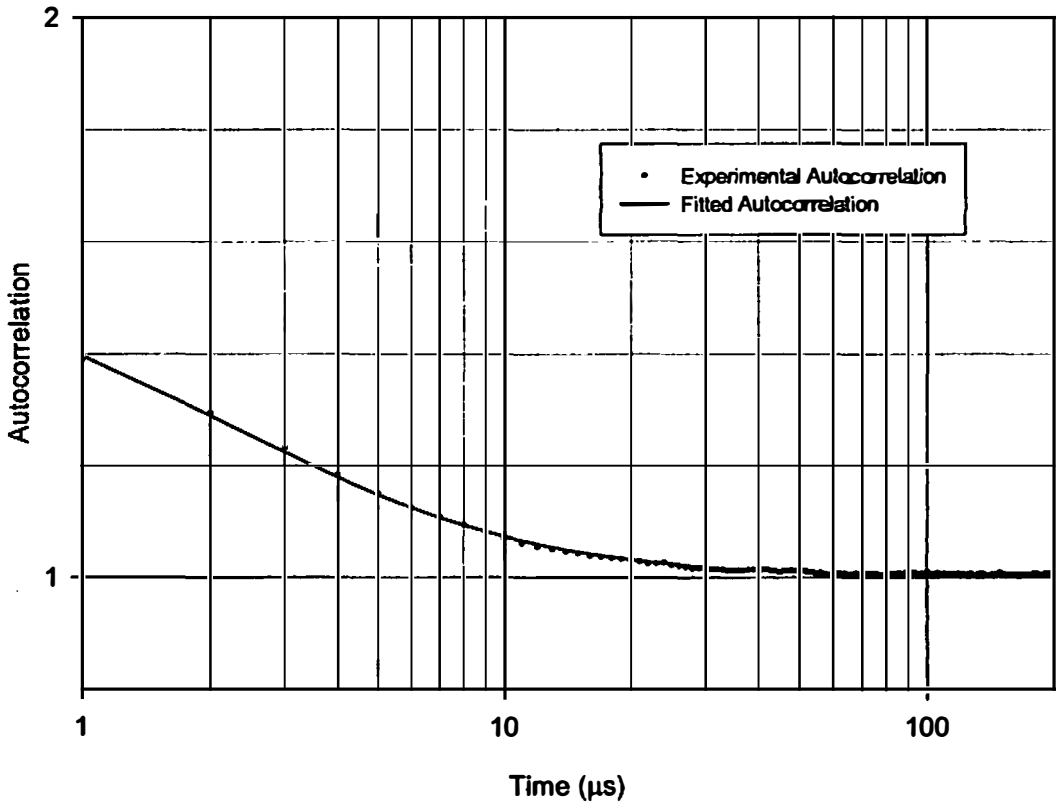

Figure 5.4: Autocorrelation fitting, 10^{-9}M sample

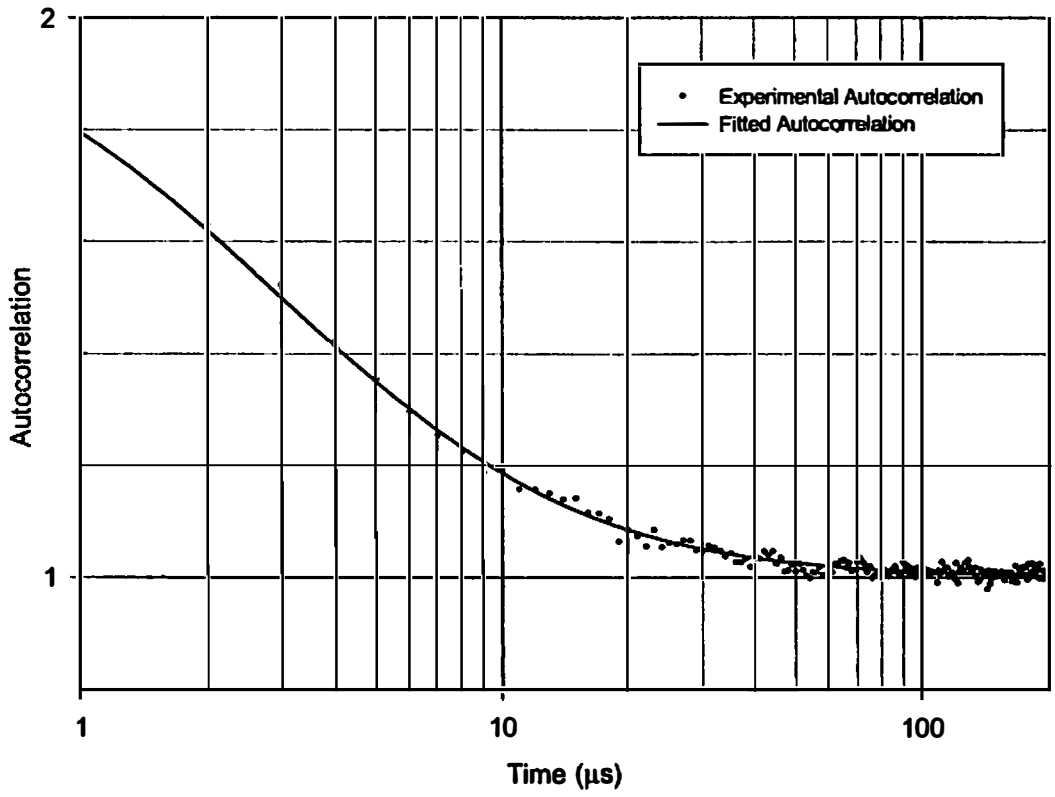

Figure 5.5: Autocorrelation fitting, 10^{-11}M sample

Dr. L. Davis indicate that the increase in background count rate, which accompanies increased laser power, causes the peak in the autocorrelation function to decrease in amplitude.]

Also of interest is the determination of the rotational diffusion coefficient. Our experiments focused primarily on the translational diffusion coefficient, but to completely characterize a molecule the rotational diffusion coefficient is also necessary.

5.4 Fluorescence quenching experiment using the UTSI instrument

The experiments on fluorescence quenching were performed by first binding fluorescent molecules to protein molecules, then examining different concentrations of the resulting solution in the microscope. Once this procedure was completed, a sample of the same solution to which a fluorescence quencher had been added was tested, using the same concentrations as before. A number of these studies were performed, the result of one such series will be given to illustrate the use of the UTSI instrument.

In Figure 5.6, the top curve on the graph is the plot of cumulative photon bursts versus peak amplitude of an unquenched fluorophore. The bottom curve is a plot of the cumulative photon bursts of the same fluorophore with a fluorescent quencher

Table 5.3: Autocorrelation fitting coefficients (UTSI instrument)

Sample	a_1	a_2 (s^{-1})	a_3
10^{-11} M	1.08	0.06	1.01
10^{-9} M	1.05	0.08	1.00

bound to it. Fluorescence quenching will affect a fluorophore in one of two ways: all the molecules of the fluorophore may give smaller photon bursts as a result of the quencher, or fewer molecules may give photon bursts. The graph illustrates the effect of a particular fluorescent quencher on a particular fluorescent probe. A large number of similar experiments were performed to determine the effects of particular quenching agents bound to specific fluorophores.

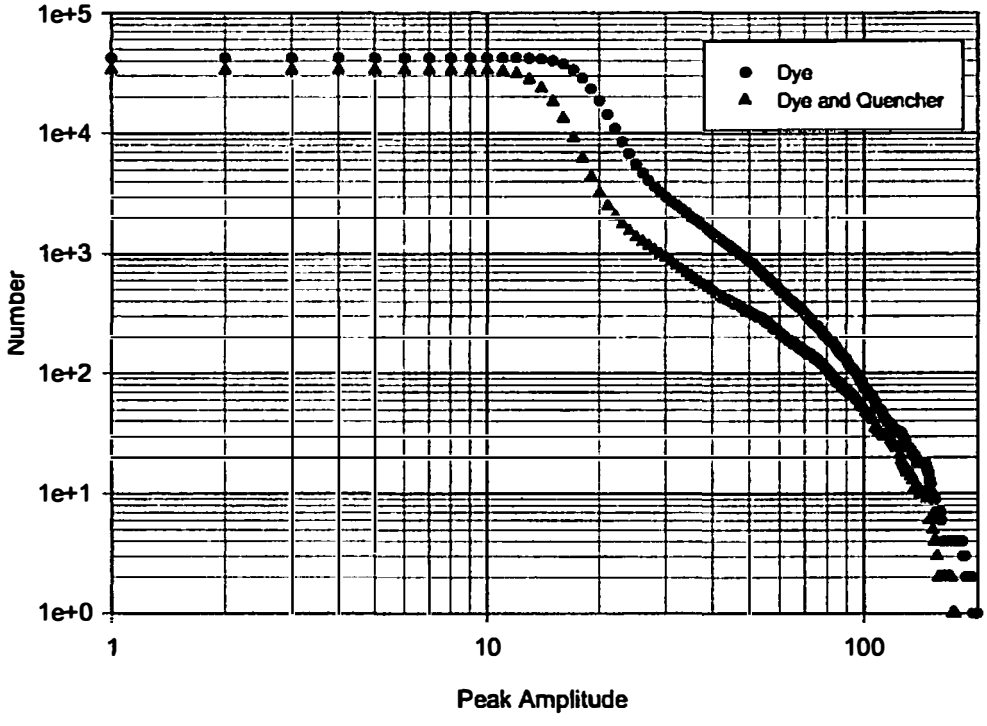

Figure 5.6: Fluorescence quenching - cumulative histogram of burst amplitudes

Chapter 6

Single-molecule imaging

In addition to the work I conducted with the confocal epi-illumination microscopes, I also worked on a separate LI-COR research contract to construct a total-internal-reflection (TIR) microscope to detect fluorescence from single molecules. Our objectives for this project were to image individual single-chromophore molecules in free solution using TIR, to evaluate different microscope objectives, and to compare the performance of two different camera systems.

In TIR fluorescence microscopy, laser light at an angle above the critical angle is incident upon a coverslip upon which a sample is placed, as shown in Figure 6.1. The light totally reflects at that interface, and an evanescent wave is generated within the sample, so that fluorophores near the interface are excited. The critical angle is determined by Snell's Law,

$$\theta_c = \sin^{-1}\left(\frac{n_1}{n_3}\right) , \tag{6.1}$$

where n_1 and n_3 are the indices of refraction for the prism and the liquid solution. For

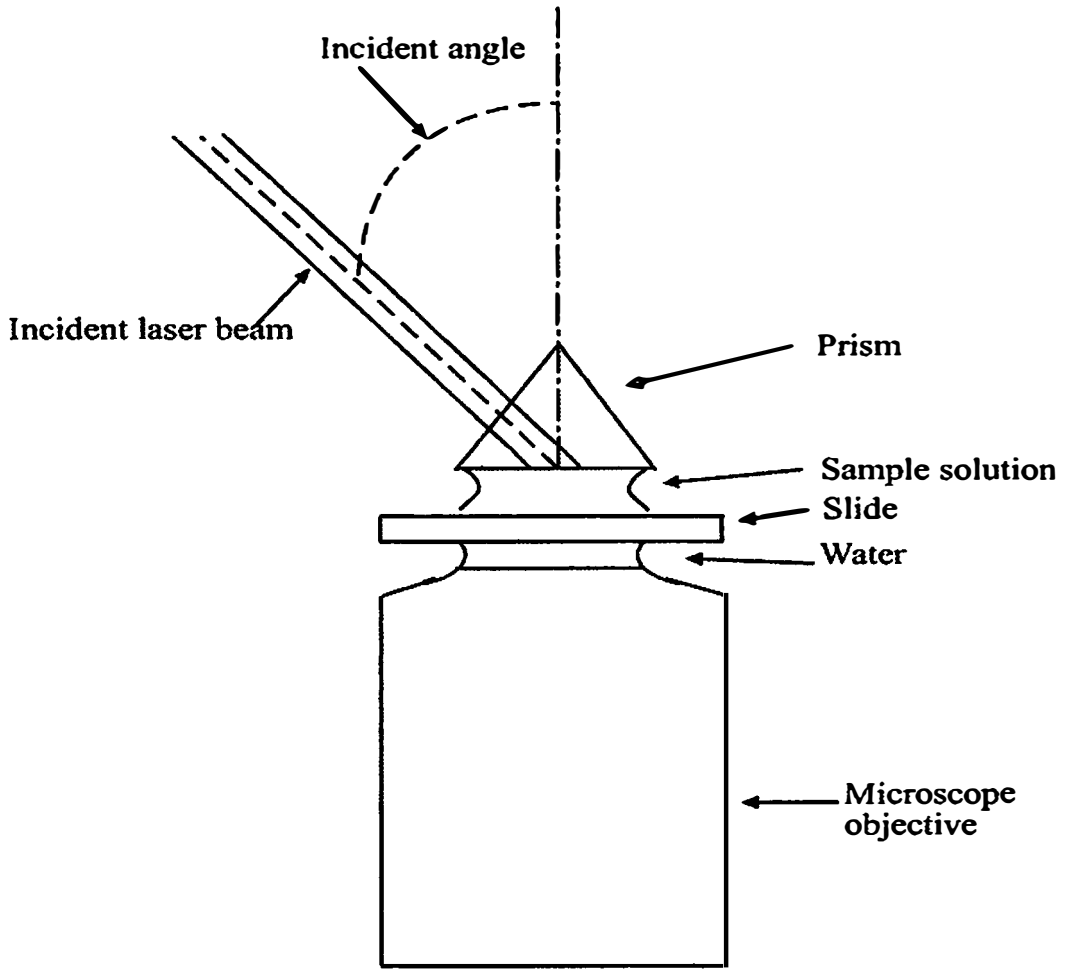

Figure 6.1: Total-internal-reflection microscopy

a water/fused-silica interface, $\theta_c = 65.7°$.

The evanescent wave has an intensity of

$$I(z) = I_0 \exp\left(\frac{-z}{d}\right) , \tag{6.2}$$

where the penetration depth d is given by

$$d = \frac{\lambda_0}{4\pi} \left(n_3^2 \sin^2\theta - n_1^2\right)^{-\frac{1}{2}} . \tag{6.3}$$

Our initial experiments utilized the same argon/krypton ion laser as used with the LI-COR confocal epi-illumination microscope. A Zeiss Axovert inverted microscope was used as a platform for the optics, and the microscope stage was modified so that the laser beam could be directed to the sample. The microscope was fitted with two camera mounts. The same arrangement of filters was used to minimize background from Rayleigh and Raman scatter. Initial experiments were conducted using solutions of SR101.

Originally we planned to compare the performance of a Princeton PentaMax intensified CCD camera with that of an Hamamatsu C2400 photon counting camera system. Due to reliability problems with the particular PentaMax camera we were using, we obtained a Princeton MicroMax back-illuminated CCD camera on loan from Princeton. We found that the back-illuminated CCD camera was apparently sufficient to image single molecules. The results of these experiments were published in References [14] and [15].

List of References

Bibliography

[1] T. Hirschfeld. Optical microscopic observation of single small molecules. *Applied Optics*, 15(12):2965–2966, December 1976.

[2] D. Nguyen and R. Keller. Detection of single molecules of phycoerythrin in hydrodynamically focused flows by laser-induced fluorescence. *Analytical Chemistry*, 59: 2158, 1987.

[3] E. Shera, N. Seitzinger, L. Davis, R. Keller, and S. Soper. Detection of single fluorescent molecules. *Chemical Physics Letters*, 174(6):553–557, 23 November 1990.

[4] L. Li and L. Davis. Single photon avalanche diode for single molecule detection. *Review of Scientific Instruments*, 64(6):1524–1529, 1993.

[5] Li Li Qianq. *Single Molecule Detection in Solution.* PhD thesis, University of Tennessee, Knoxville, Tennessee, May 1994.

[6] Dennis H. Bunfield. Simulation of a single molecule detection experiment. Master's thesis, University of Tennessee, May 1997.

[7] Yuxing Sun. *Analysis of Ultra-sensitive Fluorescence Experiments.* PhD thesis, University of Tennessee, May 1997.

[8] William T. Silvfast. *Laser Fundamentals*, chapter 5, page 143. Cambridge University Press, 1996.

[9] Joseph P. Lakowicz. *Principles of Fluorescence Spectroscopy*, pages 5–6. Kluwer Academic/Plenum Publishers, New York, NY, 2nd edition, 1999.

[10] S.R. Aragon and R. Pecora. Fluorescence correlation spectroscopy as a probe of molecular dynamics. *Journal of Chemical Physics*, 64(4):1791–1803, February 1976.

[11] J. Widengren, R. Rigler, and Ü. Mets. Triplet-state monitoring by fluorescence correlation spectroscopy. *Journal of Fluorescence*, 4(3):255–258, 1994.

[12] S.A. Soper, E.B. Shera, L.M. Davis, H.L. Nutter, and R.A. Keller. The photophysical constants of several fluorescent dyes pertaining to ultrasensitive fluorescence spectroscopy. *Photochem. and Photobiol.*, 57:972, 1993.

[13] Thorsten Wohland, Rudolf Rigler, and Horst Vogel. The standard deviation in fluorescence correlation spectroscopy. *Biophys. J.*, 89(6):2987–2999, June 2001.

[14] W. Parker, L. M. Davis, J.G.K. Williams, L.R. Middendorf, and G. Bashford. Single-molecule imaging in solution with total internal reflection. *Conference on Lasers and Electro-Optics*, pages 502–3, May 7-12 2000. San Francisco.

[15] L.M. Davis, W.C. Parker, D.A. Ball, J.G.K. Williams, et al . Imaging of single-

chromophore molecules in aqueous solution near a fused-silica interface. *Multiphoton Microscopy in the Biomedical Sciences, Proceedings of SPIE, Ammasi Periasamy, Peter T.C. So, Editors*, 4262:301–311, 2001.

Vita

Wesley C. Parker was born in Asheville, North Carolina in 1955. Prior to returning to the University of North Carolina at Asheville to complete his B.S. in Physics, he was employed for 12 years as the service and support manager for a large computer retail store in Asheville, NC. He received a B.S. in physics at UNCA in 1998. From there he went to the University of Tennessee Space Institute, where he will receive an M.S. in physics in 2002.